Density-matrix renormalization group studies of metal-halogen chains within a two-band extended Peierls-Hubbard model

1999 J. Phys.: Condens. Matter 11 2395

(http://iopscience.iop.org/0953-8984/11/11/010)

J. Phys.: Condens. Matter **11** (1999) 2395–2412. Printed in the UK PII: S0953-8984(99)96407-X

Density-matrix renormalization group studies of metal–halogen chains within a two-band extended Peierls–Hubbard model

Y Anusooya†, Swapan K Pati† and S Ramasesha†‡

† Solid State and Structural Chemistry Unit, Indian Institute of Science, Bangalore 560 012, India
‡ Jawaharlal Nehru Centre for Advanced Scientific Research, Jakkur Campus, Bangalore 560 064, India

Received 31 July 1998, in final form 11 January 1999

Abstract. The phase diagram of halogen-bridged mixed-valence metal complexes (MX) has been studied using a two-band extended Peierls–Hubbard model employing the recently developed density-matrix renormalization group method. We present the energies, charge- and spin-density distributions, bond orders, and charge–charge and spin–spin correlations, for the ground state, for different parameters of the model. The effects of bond alternation and site-diagonal distortion on the ground-state properties are considered in detail. We observe that the site-diagonal distortion plays a significant role in deciding the nature of the ground state of the system. We find that while the charge-density-wave (CDW) and bond-order-wave (BOW) phases can coexist, the CDW and SDW (spin-density-wave) phases are mutually exclusive in most cases. We have also studied the doped MX chains both with and without bond alternation and site-diagonal distortion in the CDW as well as SDW regimes. We find that the additional charges in the polarons and bipolarons for hole doping are confined to a few sites, in the presence of bond alternation and site-diagonal distortion. For electron doping, we find that the additional charge(s) is (are) smeared over the entire chain length, and although the energetics implies a disproportionation of the negatively charged bipolaron, the charge- and spin-density distributions do not reflect this. A positively charged bipolaron disproportionates into two polarons in the SDW region. There is also bond-order evidence for compression of the bond length for the positively charged polaronic and bipolaronic systems and an elongation of the bonds for systems with negatively charged polarons and bipolarons.

1. Introduction

The halogen-bridged mixed-valence metal complexes (HMMC) are quasi-one-dimensional chains that exhibit both Peierls distortion and mixed valency. This is attributed to the presence of strong electron–electron interactions as well as strong electron–lattice interactions. Additionally, the degeneracy of the ground state of the HMMC chains supports solitonic excitations as in polyacetylenes. These aspects of HMMCs have resulted in considerable theoretical and experimental focus in recent times [1–6].

The HMMCs are composed of transition metal (M) ions which are bridged by halide (X) ions. Each metal ion is surrounded by four monodentate ligand molecules such as ethylamine (L), or two bidentate ligand molecules such as ethylenediamine and cyclohexanediamine (L_2). Symbolically, HMMCs can be represented as $[M^{3-\rho}L_4][M^{3+\rho}X_2L_4]Y_4$, where M can be Pt, Pd or Ni, and X can be Cl, Br or I; ρ denotes the deviation of the metal valency from the average value of +3; and Y is a counter ion such as X^- or ClO_4^- for charge neutrality. The d_{z^2} orbital on the metal ion is singly occupied when its oxidation state is +3. Along the M–X

0953-8984/99/112395+18$19.50

backbone, the electrons are delocalized due to the overlap of the d_{z^2}(M) and p_z(X) orbitals. If the electron–electron interactions were weak compared to the electron–phonon interactions, the diagonal electron–lattice interactions would dominate. This would result in a Jahn–Teller distortion of opposite phases at successive metal-ion sites. The metal-ion site at which the d_{z^2} orbital is stabilized would be doubly occupied while that at the adjacent metal site would be empty leading to a CDW state. In the opposite limit, the strong electron–electron interactions force single occupancy of the metal d_{z^2} orbitals and the chain would be undistorted as there is no electronic stabilization associated with the distortion due to single occupancy of the metal orbitals. In this limit, a SDW state would result. As platinum is a 5d system, the d orbitals are more diffused resulting in weaker electron–electron interactions and, indeed, the broken-symmetry state observed in the Pt complexes is usually a CDW state. At the other end is the nickel system with compact d orbitals and one usually observes SDW states in the Ni complexes. The amplitude of these CDW or SDW distortions can be tuned continuously by changing the metal ion, the halide ion, the ligand, or the counter ions.

The CDW ground state in these systems has two degenerate configurations and hence there is a possibility of soliton-like excitations, besides polaronic excitations. The solitonic states in the MX chains are more localized and are believed to be longer lived than the solitons in polyacetylene chains. In the halogen-bridged mixed-valence platinum complexes (HMPC) [5], evidence for midgap absorption, associated with solitons, comes from the high-pressure studies of the optical spectra, wherein a band at half the charge-transfer excitation energy is found on application of pressure. IR and Raman studies of a series of HMMCs with decreasing metal–metal distances have also been carried out to simulate pressure and determine several microscopic parameters essential for theoretical modelling of the PtCl chains [7]. The electrical conductivity and electron spin-resonance (esr) studies [8] of halogen-doped HMPC systems show that for low doping concentrations, polarons are formed which lead to enhanced conductivity, and the charge carriers are found to have a spin. At increased dopant levels, the esr intensity reduces although the conductivity increases. Furthermore, optical absorption studies show the appearance of peaks below the optical gap. Hence, these studies suggest that two positively charged polarons yield either two positively charged solitons or a bipolaron, both of which do not have a spin. Photoinduced IR absorption studies [9] on HMPC systems with weak interchain interactions have shown evidence for photogenerated solitonic states, besides polaronic states. For large interchain coupling, the energy of formation of solitons is high and the midgap absorption band in such systems was absent, although the polaronic absorptions could be observed in these systems.

The MX chains were modelled by using a half-filled single-band Hubbard–Peierls model including nearest-neighbour electron–electron interactions by many authors [4, 10–12]. Nasu, in the mean-field limit, obtained a phase diagram for the nature of the ground state, in the parameter space of U, the on-site electron correlation strength, V, the nearest-neighbour electron–electron interaction parameter, and S, the strength of site-diagonal electron–phonon coupling. The mean-field phase diagram showed regions where CDW and SDW ground states exist as well as regions of coexistence of these two phases. It was further shown, within the mean-field theory for electrons and an adiabatic approximation for the phonons, that the origin of the photoinduced absorption was a distant hole polaron or an electron–polaron pair in the excited state of the MX chain. However, this model, apart from within the approximation for which it was solved, was quite inadequate due to the neglect of the p_z orbitals on the halogen sites. Ichinose [13] mapped the model to an anisotropic spin chain, in the limit of small on-site correlations and adiabatic electron–phonon coupling, to describe the topological excitations of the MX chain. Onodera [14] considered the continuum limit of the Ichinose model and showed that it leads to the Takayama–Lin–Liu–Maki model, which is also the continuum limit

of the discrete Su–Schreiffer–Heeger (SSH) model. He showed that the MX chains can support solitons as in polyacetylene. A model similar to the SSH model was studied by Baeriswyl and Bishop [15] who showed the existence of a charge-transfer state in the limit of strong electron–phonon interactions. The intrinsic defect states such as the polarons, bipolarons, and solitons, in this limit, were observed to be strongly localized.

Tinka Gammel *et al* first modelled the MX chains by employing a two-band U–V model (consisting of the metal d_{z^2} orbital and the halogen p_z orbital) at three-quarters filling. This model was studied by them in different approximations. In the period-4 case, they observed that the bond-order wave (BOW) phase exists only in a very small region near the point where the site energies of M and X are zero, unlike in the single-band model where the BOW is found over a wide range of parameter values. Moreover, they characterized the lowest state in that region as being of mixed CDW/BOW character. They also predicted long-period charge-density-wave ground states in the system, from an analysis of the model in the localized limit. They studied the topological excitations of the model, treating the lattice in the adiabatic approximation and the electron–electron interactions in the Hartree–Fock (both restricted and unrestricted) approximation for various parameter values to characterize these excitations in different systems. For small MX chains, they went beyond the Hartree–Fock approximation and studied the properties of the chain by employing exact-diagonalization methods. They also studied the model including the phonon dynamics but treating the electron–electron interactions in the mean-field limit. For small Hubbard interaction strengths, perturbation theory was employed to study the model. Huang and Bishop [3] studied the two-band model both in the mean-field and random-phase approximations to study the lattice- and spin-polaronic defects in Ni complexes. They found relative lattice distortion around the defect centre besides the charge or spin disproportionation. The effect of interchain interactions on the nature of the ground state and also on the energy gaps in the system were studied by including them self-consistently in finite-MX-chain calculations, within a two-band model [16]. The effect of interchain interactions on the stability of nonlinear lattice relaxation was considered by Mishima [17] in the mean-field approximation within the one-band extended Hubbard–Peierls model. Sun *et al* [18] employed a one-band model and in the mean-field approximation showed that the electron–electron interaction reduces the CDW gap in MX complexes. There is also an all-electron local density approximation calculation for MX chains which focuses on the band-gap, dimerization, and SDW instabilities in these compounds [19].

All of the studies so far carried out on the MX chain systems suffer from the disadvantage that they treat electron–electron interactions in the mean-field approximation, except in the case of small chains where model exact solutions are obtained. The exact studies on small chains are often inconclusive due to finite-size effects. However, the recently developed density-matrix renormalization group (DMRG) method has proved to be very accurate for quasi-one-dimensional systems [20]. In this paper, we report results of our extensive investigations of the MX chain systems employing the DMRG method. We have studied the MX chains with up to 70 sites (35 MX units), employing the two-band extended Peierls–Hubbard model. We have studied the neutral as well as charged MX chains to understand the properties of the ground state as well as the photogenerated gap states for many values of the model parameters. Besides energies, we have studied the charge and spin correlations in the system, the charge and spin densities, as well as bond orders, to properly characterize the ground states in different regions of the parameter space.

The paper is organized as follows. In the next section we introduce the model Hamiltonian and the DMRG method as applied to the MX chains. In the third section, we discuss results for the ground state of the neutral and doped systems. We end the paper with a summary of our findings.

2. The model Hamiltonian and the DMRG method

We have studied the HMMC systems employing the U–V–δ model. The Hamiltonian of this model, $\hat{H}$, for the metal–halogen chain can be written as a sum of the noninteracting term, $\hat{H}_0$, which includes the renormalized static electron–lattice interactions and an electron–electron interaction term, $\hat{H}_1$, as given by

$$\hat{H} = \hat{H}_0 + \hat{H}_1 \tag{1}$$

$$\hat{H}_0 = \sum_{i=1}^{N}\sum_{\sigma} t_i[a^{\dagger}_{\mathrm{X},i\sigma}a_{\mathrm{M},i\sigma} + a^{\dagger}_{\mathrm{M},i\sigma}a_{\mathrm{X},i+1\sigma} + \mathrm{h.c.}] + \sum_{i=1}^{N}\sum_{\sigma}[\epsilon_{\mathrm{M},i}a^{\dagger}_{\mathrm{M},i\sigma}a_{\mathrm{M},i\sigma} + \epsilon_{\mathrm{X},i}a^{\dagger}_{\mathrm{X},i\sigma}a_{\mathrm{X},i\sigma}] \tag{2}$$

$$\hat{H}_1 = \sum_{i=1}^{N} U_{\mathrm{M}}\frac{\hat{n}_{\mathrm{M},i}(\hat{n}_{\mathrm{M},i}-1)}{2} + \sum_{i=1}^{N} U_{\mathrm{X}}\frac{\hat{n}_{\mathrm{X},i}(\hat{n}_{\mathrm{X},i}-1)}{2} + \sum_{i=1}^{N} V_i[\hat{n}_{\mathrm{M},i}\hat{n}_{\mathrm{X},i+1} + \hat{n}_{\mathrm{X},i}\hat{n}_{\mathrm{M},i}] \tag{3}$$

where t_i is $t(1-(-1)^{(i)}\delta)$. The summations run over all the N MX pairs, and the upper limit of the summation is chosen to reflect the open boundary condition corresponding to a chain. $a^{\dagger}_{\mathrm{X},i\sigma}$ ($a^{\dagger}_{\mathrm{M},i\sigma}$) creates an electron with spin σ in the halogen (metal) orbital in the ith unit cell, and $a_{\mathrm{X},i\sigma}$ ($a_{\mathrm{M},i\sigma}$) is the adjoint of the corresponding creation operator. The operators $\hat{n}_{\mathrm{X},i}$ ($\hat{n}_{\mathrm{M},i}$) are the number operators for the halogen (metal) orbital in the ith unit cell. $\epsilon_{\mathrm{M},i}$ ($\epsilon_{\mathrm{X},i}$) is the site energy of the metal (halogen) orbital in the ith unit cell. U_{M} (U_{X}) is the on-site electron–electron repulsion parameter for the metal (halogen) orbital. The nearest-neighbour electron–electron interaction terms V_i are calculated using the Ohno [21] interpolation scheme:

$$V_i = 14.397[(28.794/(U_{\mathrm{M}} + U_{\mathrm{X}}))^2 + r^2]^{-1/2} \tag{4}$$

where r is the distance between the nearest neighbours of the MX chain. The distance r between the pairs depends on the alternation parameter δ. When the bond alternation parameter, δ, is zero, the nearest-neighbour distance is fixed at 2.447 Å. All of the parameters are defined in units of the uniform transfer integral t, whose absolute value has been assumed to be 2.0. The sign of the transfer integral is negative for an X–M bond (with the halogen on the left) and is positive for an M–X bond. This accounts for the alternating sign in the overlap of the p_z–d_{z^2} orbitals of the halogen and the metal ions.

We have employed the DMRG method to obtain the ground-state properties of the above Hamiltonian for large N ($\leqslant$35) where N is the number of MX pairs. In the DMRG method for the MX chains, we start with two MX units (four sites) and obtain the ground state of this cluster with six electrons corresponding to three-quarters filling by an exact-diagonalization procedure. We now imagine the chain to be built up of two halves, namely the left-hand half and the right-hand half. We construct the reduced many-body density matrix of the left-hand half, $\rho^{(2)}_{0,\mathrm{L}}$, in the basis of the Fock-space states of the left-hand half of the chain from the ground-state eigenfunction by integrating over the Fock-space states on the right-hand half as

$$(\hat{\rho}^{(2)}_{0,\mathrm{L}})_{\mu\nu} = \sum_{\mu'} C_{\mu\mu'}C_{\nu\mu'} \tag{5}$$

where $|\mu\rangle$ and $|\nu\rangle$ are the Fock-space states of the left-hand half of the chain and $|\mu'\rangle$ the Fock-space states of the right-hand half of the chain. $C_{\mu\mu'}$ is the coefficient associated with direct-product functions $|\mu\rangle$ and $|\mu'\rangle$ in the ground-state eigenfunction. The dimensionality of the Fock space $|\mu\rangle$ for a system consisting of n units is $l = 4^{2n}$. The density matrix is simultaneously block diagonal in both the particle-number sector and in the M^{L}_s-sector where M^{L}_s is the z-component of the total spin of the left-hand-half block. We take advantage of this while diagonalizing the density matrix by diagonalizing each of the blocks independently. This

also allows us to label each density-matrix eigenvector with the particle number, p_{L}, in addition to M_s^{L}. After diagonalization, the Fock space on the left is truncated by retaining only m of the density-matrix eigenstates corresponding to the m highest density-matrix eigenvalues. If we had retained all l density-matrix eigenvectors to serve as basis functions of the Fock space of the left-hand half, we would have merely effected a unitary transformation of the basis functions. The $l \times l$ Hamiltonian matrix $\hat{H}_{\mathrm{L}}(n)$ for the left-hand part of the chain is obtained in the basis of the Fock-space states. This matrix $\hat{H}_{\mathrm{L}}(n)$ is renormalized using the matrix $\hat{O}_{\mathrm{L}}(n)$ whose columns are the m eigenvectors of the corresponding $l \times l$ density matrix. Thus the transformation matrix $\hat{O}_{\mathrm{L}}(n)$ is an $m \times l$ matrix. The renormalized Hamiltonian matrix $\tilde{H}_{\mathrm{L}}(n)$ is given by

$$\tilde{H}_{\mathrm{L}}(n) = \hat{O}_{\mathrm{L}}^{\dagger}(n)\hat{H}_{\mathrm{L}}(n)\hat{O}_{\mathrm{L}}(n). \tag{6}$$

The renormalized left-hand Hamiltonian matrix is now an $m \times m$ matrix representation of the left-hand-half Hamiltonian in the basis of the density-matrix eigenvectors. The operators $a_{\mathrm{M},i}^{\dagger}$ and $a_{\mathrm{X},i}^{\dagger}$, and $\hat{n}_{\mathrm{M},i}$ and $\hat{n}_{\mathrm{X},i}$ corresponding to each site in the left-hand part of the chain are also obtained as matrices in the basis of the Fock space $|\mu\rangle$, and are later renormalized to obtain renormalized matrices in the basis of the eigenvectors of the density matrix of the corresponding half-chains, in a manner similar to the method of construction of $\tilde{H}_{\mathrm{L}}(n)$. The density matrix, the transformation matrix $\hat{O}_{\mathrm{R}}(n)$, the renormalized Hamiltonian matrix $\tilde{H}_{\mathrm{R}}(n)$ for the right-hand part, as well as the renormalized second-quantized site operators for the right-hand part are all obtained analogously. Unlike in the calculations involving spin chains and Hubbard chains [22], the MX chains do not have reflection symmetry, and all of the quantities should be calculated separately for the right-hand and left-hand halves of the chain.

To get the Hamiltonian for the system with $n+1$ unit cells, a MX unit is added in the middle of the chain. The Hilbert space of the new Hamiltonian matrix corresponding to $n+1$ unit cells is the direct product of m states, $|\mu\rangle$ from the left-hand block and $|\mu'\rangle$ from the right-hand block, and four states, $|c\rangle$ or $|c'\rangle$ (corresponding to $|0\rangle$, $|\downarrow\rangle$, $|\uparrow\rangle$, and $|\uparrow\downarrow\rangle$ configurations at the new site) from each of the newly added unit cells, with the restriction that the total M_s-value for the full chain is equal to the desired value and that the total system is three-quarters filled.

The Hamiltonian for $(n+1)$-unit-cell system can be written as

$$\begin{aligned}\hat{H}(n+1) = {} & \tilde{H}_{\mathrm{L}}(n) + \tilde{H}_{\mathrm{R}}(n) + \hat{n}_c\epsilon_c + \hat{n}_{c'}\epsilon_{c'} + \frac{U_c}{2}\hat{n}_c(\hat{n}_c - 1) + \frac{U_{c'}}{2}\hat{n}_{c'}(\hat{n}_{c'} - 1) \\ & + t_n[\tilde{a}_{\mathrm{L}}^{\dagger}(n)a_c + \text{h.c.}] + t_{n+1}[a_c^{\dagger}a_{c'} + \text{h.c.}] + t_{n+1}[a_{c'}^{\dagger}\tilde{a}_{\mathrm{R}}(n) + \text{h.c.}] \\ & + V_n\tilde{n}_{\mathrm{L}}(n)\hat{n}_c + V_{n+1}\hat{n}_c\hat{n}_{c'} + V_{n+1}\hat{n}_{c'}\tilde{n}_{\mathrm{R}}(n)\end{aligned} \tag{7}$$

where the operators $\tilde{a}_{\mathrm{L}}^{\dagger}(n)$, $\tilde{a}_{\mathrm{R}}^{\dagger}(n)$, and their adjoints, as well as $\tilde{n}_{\mathrm{L}}(n)$, $\tilde{n}_{\mathrm{R}}(n)$, are the renormalized operators expressed in the truncated density-matrix eigenvector basis. The operators $\hat{a}_c^{\dagger}$ ($\hat{a}_{c'}^{\dagger}$) and their adjoints as well as $\hat{n}_c$ ($\hat{n}_{c'}$) are expressed as matrices in the Fock-space basis. The matrix representation of the Hamiltonian $\hat{H}(n+1)$ in the direct-product basis is obtained as the appropriate direct product of the operators occurring in the Hamiltonian.

The eigenvalues and eigenvectors for these $n+1$ unit cells are obtained, and the reduced density matrices for the left-hand and right-hand halves of the chain, each with $n+1$ sites, are constructed from the ground-state eigenfunction. In the next iteration, the procedure is repeated by adding an XM unit in the middle of the chain. We have to add MX and XM units alternately in the middle of the chain so that the successive sites of the full chain at any iteration are not occupied by like ions.

When alternation is introduced, the unit cell consists of two MX units with one metal atom having two short M–X bonds and another having two long M–X bonds, i.e.

$$[\text{–M–X—M—X–}]_n.$$

We start our calculations with a four-site MX system in the geometry corresponding to M–X—M–X. To obtain the correct geometry of the alternated system, we require systems with $4n + 2$ sites (n integer). Thus, while at the end of each DMRG iteration we obtain results for the proper MX system in the absence of static lattice distortion, in the distorted MX chain, only at the end of an odd-numbered iteration do we obtain the desired system. The halogen on-site energy, ϵ_{X}, is negative, while the metal on-site energy, ϵ_{M}, is positive when the metal has two short bonds with the halogens and is negative when it has two long bonds.

The lack of reflection symmetry of the MX chain leads to a modified DMRG algorithm for finite systems. Each iteration in the finite DMRG procedure goes through in two steps. In the first step the left-hand part of the system is increased in size by one site while the corresponding right-hand part is decreased in size by one site as in the usual finite-size DMRG algorithm [20]. On obtaining $\rho_{0,\mathrm{L}}^{(2N-4)}$, the density matrix of the $(2N-4)$-site left-hand part in the $2N$-site chain system (the superscript in parentheses refers to the iteration index in the finite-system algorithm), we progressively rebuild the desired $2N$-site system (N MX units), increasing the size of the right-hand part while correspondingly reducing the size of the left-hand part. In this process, we rebuild the density matrix of the right-hand part for every size as the density matrix of the full $2N$ system. This procedure now yields $\rho_{1,\mathrm{R}}^{(N-1)}$ and is continued till we obtain $\rho_{1,\mathrm{R}}^{(2N-4)}$. At this stage, we reverse the process and increase the size of the left-hand part of the system from two sites while simultaneously decreasing the size of the right-hand part until we construct the $\rho_{1,\mathrm{L}}^{(N-1)}$ density matrix. Now, employing $\rho_{1,\mathrm{L}}^{(N-1)}$ and $\rho_{1,\mathrm{R}}^{(N-1)}$, we build the full $2N$ system and obtain its desired eigenstates. This completes the first iteration of the finite DMRG procedure of the system without reflection symmetry. The whole iteration procedure is repeated now with $\rho_{1,\mathrm{L}}$ and $\rho_{1,\mathrm{R}}$ until satisfactory convergence in the energy is attained.

To check the accuracy of the DMRG procedure, we have carried out the following test. For system sizes up to seven MX units ($N = 7$), we have compared the results from DMRG calculations with exact calculations. The maximum error in the ground-state energy is of the order of 0.01%, with a DMRG cut-off of $m = 80$, and we use this value of m in all of our calculations. The dimensionality of the Hilbert space corresponding to $M_s = 0$ (the $4n$-site system) or 0.5 (the $(4n + 2)$-site system) and $N_e = \frac{3}{2}N$ varies in the range 6400 to 7000, depending upon the model parameters, for this value of m. The resulting Hamiltonian matrix is very sparse. The total number of nonzero matrix elements is $\approx 5 \times 10^5$. We exploit the sparseness of the Hamiltonian matrix to reduce the storage requirement as well as the CPU requirement by avoiding doing arithmetic with zeros. We have used the Davidson algorithm for a symmetric Hamiltonian matrix to get the lowest few eigenvalues. The Davidson algorithm, which is a hybrid of the coordinate-relaxation method and the Lanczos method, has been widely used in quantum chemical computations and is known to be both robust and rapidly convergent.

We have also compared the properties of the interacting and noninteracting DMRG ground state respectively (a) with exact properties of small interacting systems using the valence band method [23, 24] and (b) with exact properties of large noninteracting systems. The properties that we have compared are the bond orders, and the charge and spin densities (where the three-quarters filling leads to an odd-electron system). The comparisons are carried out for both neutral and doped systems. We find that the agreement between properties calculated from the DMRG and those obtained from exact cases is excellent. We note that even in the latter case the agreement between exact Hückel and DMRG Hückel calculations is very good. The checks presented above have been made by employing the infinite DMRG algorithm. We have not presented finite DMRG results for noninteracting cases as the infinite DMRG algorithm is itself in very good agreement with exact results. We also find that the finite DMRG algorithm

gives results which are not significantly different from those obtained from the infinite DMRG algorithm even in the worst cases. All of these checks provide sufficient confidence in our result to allow us to draw unambiguously some important conclusions concerning the instabilities in doped and neutral MX chains, using only the infinite DMRG algorithm.

3. Results and discussion

We have studied the ground state of the MX chains in different regions of parameter space to explore the phase transformation from the CDW phase to the SDW phase. The parameters U_M, U_X, and ϵ_M, ϵ_X characterize the metal ion and the halide ion. The orbital energy of the halide ion, ϵ_X, is specified relative to the orbital energy of the corresponding metal ion of the uniform MX chain. ϵ_X is always negative, reflecting the larger electronegativity of the halogens compared to the metal ions. In the halide series, a larger negative ϵ_X represents chloride while the least negative ϵ_X represents iodide, reflecting the electronegativity variations in the halogen group. The on-site repulsion parameter for the halide ion, U_X, is positive and decreases as we go down the series from Cl^- to I^-. The Hubbard parameter for the metal ion, U_M, decreases as we go from the row I transition elements to the row III transition elements. The parameters U_M, U_X and ϵ_X are varied from $U_M = 2.5t$, $U_X = t$, $\epsilon_X = -2t$ to $U_M = 1.5t$, $U_X = 0.5t$, $\epsilon_X = -t$ corresponding to the MX pairs NiCl to PtI respectively. The ϵ_M-values depend upon the strength of the diagonal electron–lattice coupling and so does the alternation δ in the transfer integrals. The coupling constants for the diagonal and off-diagonal couplings are assumed to be independent. Accordingly, we independently vary the transfer integrals as well as the site energy at the metal site, ϵ_M. This is one of the crucial differences between a polyene chain and the MX chain. In the former, the site-diagonal electron–phonon coupling is taken to be zero, while in the MX chains it is nonzero by virtue of the crystal-field environment provided by the halide ions surrounding the metal ions. The dimerization parameter, δ, has been varied between 0.0 and 0.2. In what follows, we first discuss the results of our study of MX chains at three-quarters filling, and then discuss our results for these chains with one and two excess (fewer) electrons.

In figure 1 we present the dependence of the ground-state energy per MX unit (ϵ_{MX}) of the MX chains for different values of δ for one set of parameters. The convergence to the

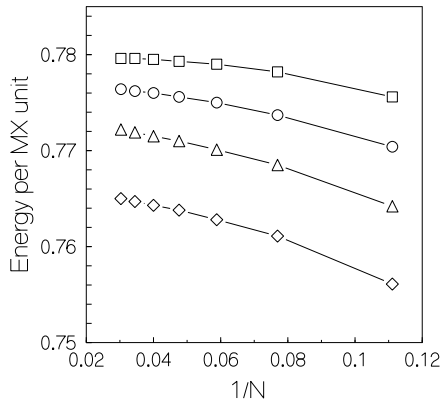

Figure 1. A plot of the energy per MX unit versus $1/N$ for different values of δ for $U_M = 1.5t$, $U_X = 0.5t$, $\epsilon_M = 0.0$, and $\epsilon_X = -t$. $\delta = 0.0$ (squares), $\delta = 0.1$ (circles), $\delta = 0.15$ (triangles), $\delta = 0.2$ (diamonds).

Table 1. Fractional stabilization of the energy defined as $(E(\delta) - E(0))/E(0)$ of MX chains with respect to uniform chains for different parameter sets. I: $U_M = 1.5t$, $U_X = 0.5t$, $\epsilon_M = 0$, $\epsilon_X = -t$; II: $U_M = 1.5t$, $U_X = 0.5t$, $\epsilon_M = 0$, $\epsilon_X = -2t$; III: $U_M = 2.5t$, $U_X = 0.5t$, $\epsilon_M = 0$, $\epsilon_X = -t$; IV: $U_M = 2.5t$, $U_X = 0.5t$, $\epsilon_M = 0$, $\epsilon_X = -2t$; V: $U_M = 2.5t$, $U_X = 0.5t$, $\epsilon_M = t$, $\epsilon_X = -2t$.

δ	I	II	III	IV	V
0.10	−0.0043	−0.0127	−0.0007	−0.0017	−0.0560
0.15	−0.0109	−0.0319	−0.0026	−0.0055	−0.0990
0.20	−0.0210	−0.0598	−0.0054	−0.0104	−0.1489

infinite-chain value is monotonic and from below. We have defined ϵ_{MX} as half the total energy difference between successive iterations which differ by two MX units. This definition corresponds to the energy of an embedded MX unit and is akin to that of the rings. It is well known that the energy per site of Hubbard, extended Hubbard, as well as spin rings converge to the limiting value from below [25]. In table 1, we have shown the dependence of the fractional stabilization of the MX chain on introducing alternation for several sets of parameters. We find that the alternation lowers ϵ_{MX} in all of the cases that we have studied, but the extent of the stabilization is insensitive to variations in U_M and ϵ_X when the diagonal electron–phonon coupling is neglected. Since the energy per MX unit cannot be reliably extrapolated to the infinite-chain limit (we do not observe saturation in energy per MX unit at 35 MX units), we do not know the functional dependence of $\Delta E(\delta) = E_\infty(\delta) - E_\infty(0)$ on δ. However, a rough estimate shows that $\Delta E(\delta) = \delta^\eta$, $\eta > 2$. This implies that the MX chain may not distort unconditionally. Our results on introducing the diagonal electron–phonon interaction along with bond alternation, δ, indicate the dominant role of electron–phonon interactions in determining the extent of bond alternation. In fact, in systems where bond alternation is indeed found, the magnitude of the alternation is very large.

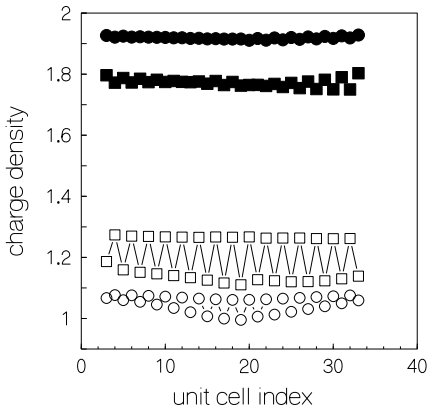

Figure 2. The charge density of M and X versus the unit-cell index. Open and filled symbols are for M and X respectively. Squares represent the charge density for $U_M = 1.5t$, $U_X = 0.5t$, $\epsilon_M = 0$, $\epsilon_X = -t$, and $\delta = 0.1$, and circles that for $U_M = 2.5t$, $U_X = 0.5t$, $\epsilon_M = 0$, $\epsilon_X = -2t$, and $\delta = 0.1$.

In figure 2 we present the charge densities at the metal and halide sites in the alternating ($\delta = 0.1$) MX chains without diagonal distortions ($\epsilon_M = 0$) for two extremal values of U_M and ϵ_X. We find that the charge densities at the metal sites are very nearly uniform in both cases. For small values of ϵ_X and U_M, the charge density in the metal orbital is larger at $\approx 1.2 \pm 0.08$, while it is more uniform, with values in the range $\approx 1.06 \pm 0.04$, for large U_M and large ϵ_X.

The charge densities at the halide sites are uniform and closer to two electrons when ϵ_X and U_M are large. While the alternation in the transfer integral along the chain seems to promote mixed valency, the large electron–electron repulsion at the metal site and the large site energy of the halogen orbital have the effect of suppressing mixed valency. This is in conformity with experiments wherein mixed valency is found in MX chains with heavier transition elements as well as heavier halogen atoms. Increasing the alternation in the transfer integral does not change the picture significantly. There is a slight increase in the amplitude of the charge-density wave in the most favourable case that we have studied, corresponding to $U_M = 1.5t$ and $\epsilon_X = -t$.

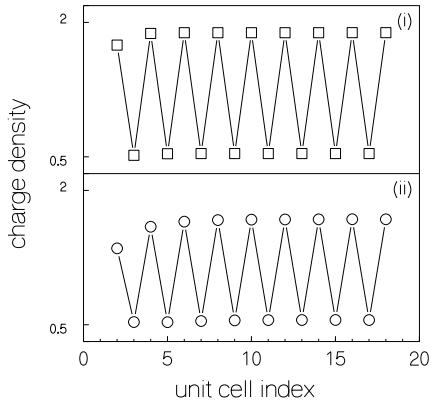

Figure 3. The charge density of M versus the unit-cell index in the presence of site-diagonal distortion. (i) $U_M = 1.5t$, $U_X = 0.5t$, $\epsilon_M = t$, $\epsilon_X = -t$, and $\delta = 0.1$ (squares). (ii) $U_M = 2.5$, $U_X = 0.5t$, $\epsilon_M = t$, $\epsilon_X = -2t$, and $\delta = 0.1$ (circles).

In figure 3, we show a plot of the charge density at metal sites in the presence of diagonal distortion ($\epsilon_M \neq 0.0$) for alternation $\delta = 0.1$ for the two extremal cases that we have studied, namely, large U_M, large ϵ_X, and small U_M, and small ϵ_X for one particular value of ϵ_M. We see a dramatic change in the charge-density distribution in both cases. In the favourable case, the disproportionation of the metal ion in the 3+ oxidation state into 2+ and 4+ oxidation states is almost complete, while even in our least favourable case, the amplitude of the CDW is quite significant. In the latter case, increasing ϵ_M increases the amplitude rapidly. This result underlines the importance of diagonal distortion in producing a CDW ground state.

The variation in bond order along the MX chain is plotted for several values of the parameters in figure 4 only for the left-hand half of the chain. The amplitude of the BOW behaves similarly to the amplitude of the CDW. The diagonal distortion has a strong effect on the BOW amplitude. Even in the most unfavourable case of $U_M = 2.5t$ and $\epsilon_X = -2t$, the BOW picks up sufficient amplitude for the site-diagonal distortion that we have considered. The earlier prediction of Tinka Gammel *et al* [1] that a BOW cannot exist for negative halide-site energy with site-diagonal distortion lowering the metal-ion-site energy is not borne out by our calculations.

The spin-density distribution shows a trend opposite to what is observed with CDW and BOW instabilities. For large U_M and large ϵ_X, in the uniform MX chain, the SDW amplitude is fairly large. Introducing off-diagonal alternation reduces the amplitude, although the alternation in the spin density still exists. However, on introducing diagonal distortion, all of the metal sites become completely nonmagnetic. This behaviour shows that when the CDW/BOW amplitude is large, the amplitude of the SDW is small. Figure 5 brings out this

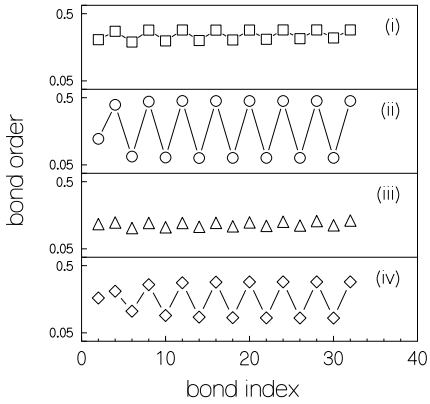

Figure 4. The bond order versus the bond index. (i) $U_M = 1.5t$, $U_X = 0.5t$, $\epsilon_M = 0$, $\epsilon_X = -t$, and $\delta = 0.1$ (squares). (ii) $U_M = 1.5t$, $U_X = 0.5$, $\epsilon_M = t$, $\epsilon_X = -t$, and $\delta = 0.1$ (circles). (iii) $U_M = 2.5t$, $U_X = 0.5t$, $\epsilon_M = 0$, $\epsilon_X = -2t$, and $\delta = 0.1$ (triangles). (iv) $U_M = 2.5t$, $U_X = 0.5t$, $\epsilon_M = t$, $\epsilon_X = -2t$, and $\delta = 0.1$ (diamonds).

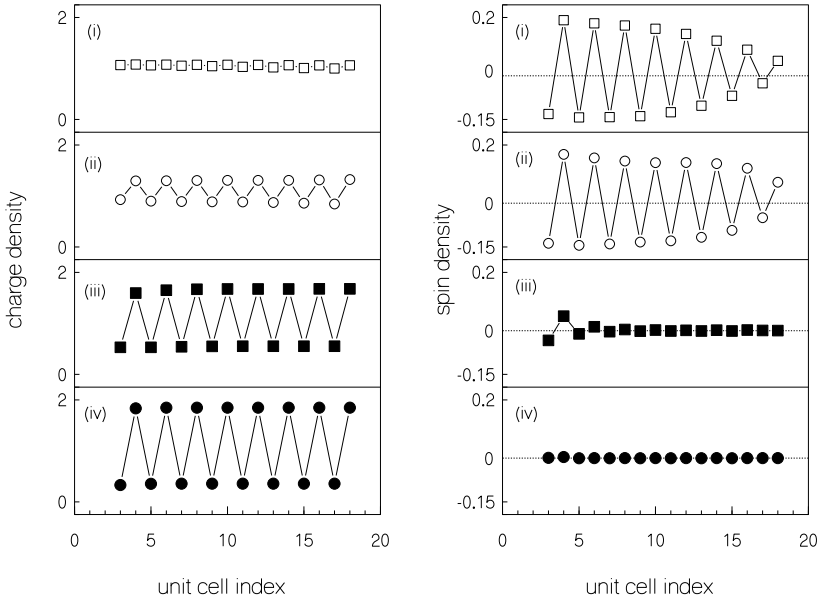

Figure 5. The variation of (a) charge densities and (b) spin densities with site-diagonal distortion, ϵ_M, versus the unit-cell index for $U_M = 2.5t$, $U_X = 0.5t$, $\epsilon_X = -2t$, and $\delta = 0.1$. (i) $\epsilon_M = 0.0$ (open squares). (ii) $\epsilon_M = 1.0$ (open circles). (iii) $\epsilon_M = 2.0$ (filled squares). (iv) $\epsilon_M = 3.0$ (filled circles).

trend by comparing the charge and spin densities at metal sites for different values of the site-diagonal distortion parameter ϵ_M. It is also interesting to note that for one set of parameter values, the CDW and the SDW phases coexist (see part (ii) of figure 5).

We have also characterized the ground state in various regimes of the parameter by studying the spin–spin and charge–charge correlation functions. Although these correlation functions

have been computed for open chains, they can be Fourier transformed, if one assumes that the correlations in the interior of the open chain are close to what would be seen in a ring. This assumption was first made by Sorenson and Affleck [26] to obtain the structure factors from open-chain DMRG calculations of spin systems. In our calculations, we have discarded the last three unit cells on either end of the chain and have assumed the correlations to have a reflection symmetry about the middle bond. This enables us to Fourier transform the correlation functions.

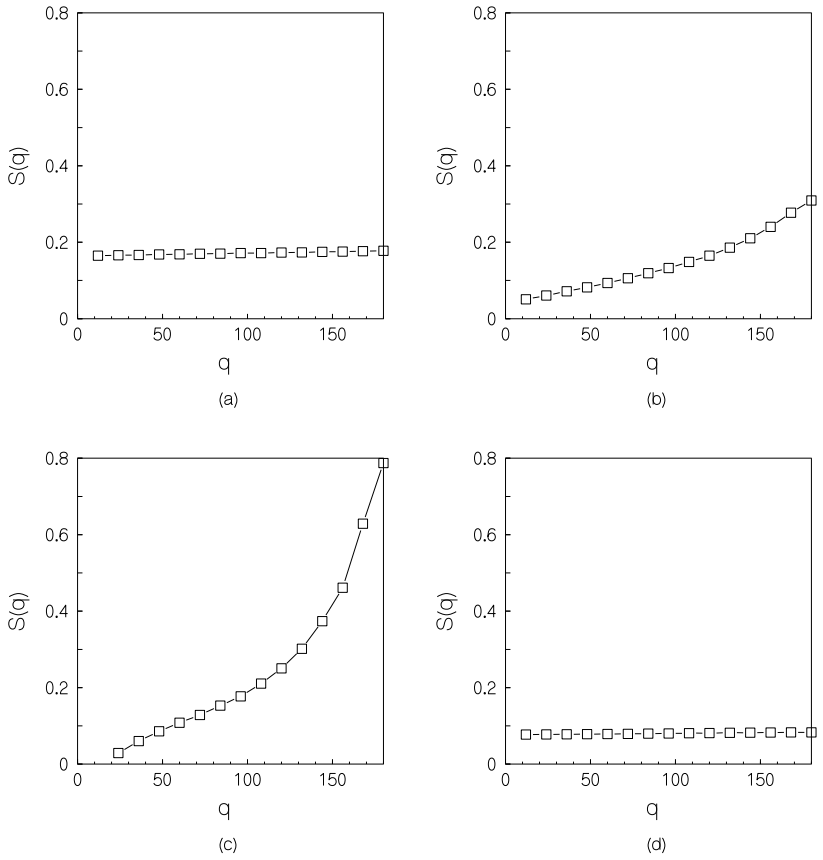

Figure 6. The spin structure factor versus the momentum, q (in degrees). (a) $U_{\mathrm{M}} = 1.5t$, $U_{\mathrm{X}} = 0.5t$, $\epsilon_{\mathrm{M}} = 0$, $\epsilon_{\mathrm{X}} = -t$, and $\delta = 0.0$. (b) $U_{\mathrm{M}} = 1.5t$, $U_{\mathrm{X}} = 0.5t$, $\epsilon_{\mathrm{M}} = 0$, $\epsilon_{\mathrm{X}} = -t$, and $\delta = 0.2$. (c) $U_{\mathrm{M}} = 2.5t$, $U_{\mathrm{X}} = 0.5t$, $\epsilon_{\mathrm{M}} = 0$, $\epsilon_{\mathrm{X}} = -2t$, and $\delta = 0.2$. (d) $U_{\mathrm{M}} = 2.5t$, $U_{\mathrm{X}} = 0.5t$, $\epsilon_{\mathrm{M}} = t$, $\epsilon_{\mathrm{X}} = -2t$, and $\delta = 0.1$.

In figure 6, we show the spin structure factor, $S(q)$, for various values of the model parameters. In the CDW phase which corresponds to small U_{M}, small ϵ_{X}, and nonzero site-diagonal distortion and alternation, we find that $S(q)$ is very small. However, for large U_{M}, large ϵ_{X}, zero site-diagonal distortion, but with nonzero δ, the structure factor is large and peaks at $q = \pi$. This result reflects the spin ordering of the ground state. The uniform structure factor in figures 6(a) and 6(d) confirms the ground state to be in a non-SDW phase. This result is also consistent with the charge and spin density, and also the bond-order data discussed above. The structure factor corresponding to the charge–charge correlation function, $\rho(q)$, shows a different behaviour. Here, for large U_{M} and large negative ϵ_{X}, the structure factor is almost

uniform and does not show any pronounced peaks. However, for small U_M, small negative ϵ_X, and nonzero site-diagonal distortion, the structure factor peaks at π corresponding to the existence of a CDW phase. The importance of the diagonal distortion is underscored by the fact that even for nonzero δ, small U_M, and small negative ϵ_X, the peak at π in the structure factor, though discernible, is not pronounced. It is also interesting to note that $\rho(q)$ shows small oscillations away from the peak at π which could be due to incipient long-wavelength CDW distortions which could have nonzero amplitude in the thermodynamic limit as suggested by Tinka Gammel *et al* [1].

3.1. MX chains marginally away from three-quarters filling

The DMRG method for MX chains cannot access the energy levels that have been studied by optical spectroscopies. The reason for this is that there are a large number of low-lying excitations in long MX chains which intrude while targeting excited states, and the absence of the symmetries in open chains rules out the possibility of avoiding the intruder states. Hence, we have been unable to study the optical properties of long MX chains by this technique. However, there is considerable interest in the photogenerated gap states which arise from the dissociation of the excitons produced in an optical experiment. These states are, typically, the positive and negative polarons and bipolarons and the charged and neutral solitons of the system. The DMRG method can easily access the polaronic and bipolaronic states. In what follows, we present results of the DMRG study of these species at representative points in the parameter space, namely $U_M = 1.5t$, $\epsilon_X = -t$ and $U_M = 2.5t$, $\epsilon_X = -2t$, corresponding to the CDW and SDW regimes. These parameters are taken together with $\epsilon_M = 0.0$ or t and $\delta = 0.1$, $U_X = 0.5t$ to explore the importance of site-diagonal distortion in the two regimes.

It is computationally prohibitive to distort doped chains self-consistently to study the formation of polarons and bipolarons. However, the bond orders of the doped chains indicate the susceptibility of the chain to distortion. Coulson's formula for polyenes, for example, gives a direct relation between bond orders and bond lengths. For small systems, our earlier studies [16], carried out incorporating the distortion of the chain self-consistently, show that the distortion given by a formula similar to Coulson's formula gives bond lengths very close to equilibrium bond lengths even at the first iteration. Therefore, the excess-charge-density distribution together with bond-order patterns in the chain will give us information about the nature of the states produced upon doping.

Since we are studying inhomogeneous system, it is important to follow the convergence of the properties with increasing system size. We first discuss the energetics of the polarons

Table 2. The energies (in units of t) for doped MX chains of 35 units with one and two holes as well as one and two electrons, for various representative parameters of the Peierls–Hubbard model. I corresponds to $U_M = 1.5t$, $U_X = 0.5t$, and $\epsilon_X = -t$, while II corresponds to $U_M = 2.5t$, $U_X = 0.5t$, and $\epsilon_X = -2t$.

	I				II			
	$\epsilon_M = 0.0$		$\epsilon_M = t$		$\epsilon_M = 0.0$		$\epsilon_M = t$	
Doping	$\delta = 0.0$	$\delta = 0.1$	$\delta = 0.0$	$\delta = 0.1$	$\delta = 0.0$	$\delta = 0.1$	$\delta = 0.0$	$\delta = 0.1$
Two holes	−9.6308	−9.7157	−9.3790	−9.1630	−12.2875	−12.3646	−13.5137	−13.4442
One hole	−4.8361	−4.8944	−4.6590	−4.5038	−6.1595	−6.2060	−6.8225	−6.7591
One electron	4.9375	4.9451	5.2900	5.3242	6.1935	6.2158	6.8850	6.9995
Two electrons	10.3529	10.3245	10.7410	10.8901	13.9677	13.9482	13.9909	14.0724

and bipolarons, for the chosen parameter set. The energy per unit cell of the doped MX chain obtained as the difference in total energy between two successive iterations converges very rapidly to the thermodynamic limit for different parameter values. For nonzero δ, the unit cell contains two MX units, and the energy per unit cell is obtained as the difference in total energies of the two successive odd iterations. In table 2 we give the energy for doping of MX chains of 35 units with one or two holes and one or two electrons. The magnitude of the doping energy increases with increase in strength of the electron correlations. The stabilization energies upon doping with one (two) hole(s) is (are) almost equal in magnitude to the energy required for creating chains doped with one (two) electron(s) respectively. Neither the bond alternation nor the site-diagonal distortion energy at the metal site have any noticeable influence on the doping energetics. However, the positively charged bipolaron and the negatively charged bipolaron are not placed symmetrically around the ground state in the energy scale. From the energetics, one can see that at larger correlation strengths, the positively charged bipolaron is less stable than two positively charged polarons. This is also true for negatively charged bipolarons irrespective of the Hubbard U. Thus, it appears from the energetics that both the positively and the negatively charged bipolarons should dissociate into two polarons.

The definitive proof for the disproportionation of the bipolarons comes from comparing the charge- and spin-density distributions at the metal sites of the bipolarons with those of the polarons bearing charges of the same sign. The charge densities at the metal site for the polarons and bipolarons are shown in figure 7. The polaron charge densities for (I) $U_{\mathrm{M}} = 1.5t$, $\epsilon_{\mathrm{M}} = 0.0$, $U_{\mathrm{X}} = 0.5t$ and $\epsilon_{\mathrm{X}} = -t$ are shown in figure 7(a), and for (II) $U_{\mathrm{M}} = 2.5t$, $\epsilon_{\mathrm{M}} = 0.0$, $U_{\mathrm{X}} = 0.5t$, and $\epsilon_{\mathrm{X}} = -2t$ they are shown in figure 7(c). The data for bipolarons for the parameter set I are shown in figure 7(b) and for the set II they are shown in figure 7(d). For the parameter set I (figures 7(a) and 7(b)), the additional charge is uniformly distributed over the entire chain for (i) the positively charged polaron/bipolaron, (ii) the neutral chain, and (iii) the negatively charged polaron/bipolaron. For the second set of parameters, i.e. at large U_{M}, we observe more localized charge distribution for both the positively charged polaron and the positively charged bipolaron. We also observe two broad peaks (figure 7(d)) in the charge distribution of the positively charged bipolaron which is indicative of disproportionation of the positively charged bipolaron into two positively charged polarons. However, in the case of the negatively charged polaron and bipolaron, the Hubbard U prevents localization of the charge. An earlier mean-field study [1] found the negatively charged polaron and bipolaron to be more localized than the positively charged polaron and bipolaron. Our DMRG results correspond to an on-site halide repulsion parameter U_{X} which is smaller than the metal on-site repulsion parameter, U_{M}, and our study should have lent more support to this difference between the hole defects and the electron defects predicted by the mean-field analysis. It appears, therefore, that the mean-field approximation gives wrong trends for charge distributions of the defects. On physical grounds, one should expect the on-site repulsions to spread out the excess negative charge more than the excess positive charge.

The evidence for the disproportionation of the positively charged bipolaron into two polarons is more pronounced when alternation in the chain is introduced (figure 8). The charge-density distribution of the polaron (figure 8(a)) shows a single hump while that for the bipolaron (figure 8(b)) shows two humps. The hole charge density is mostly confined to one sublattice of the metal ion; the one in which the metal–halogen bond is shorter accommodates the excess charge. The homogeneity of halogen charge-density distribution is not affected significantly by doping. The spin-density distribution shows the disproportionation more clearly, as seen from the two separate envelopes for the spin density in the bipolaron (figure 8(d)) compared to a single envelope in the polaron spin-density distribution (figure 8(c)). This break-up of the bipolaron is observed only for hole doping.

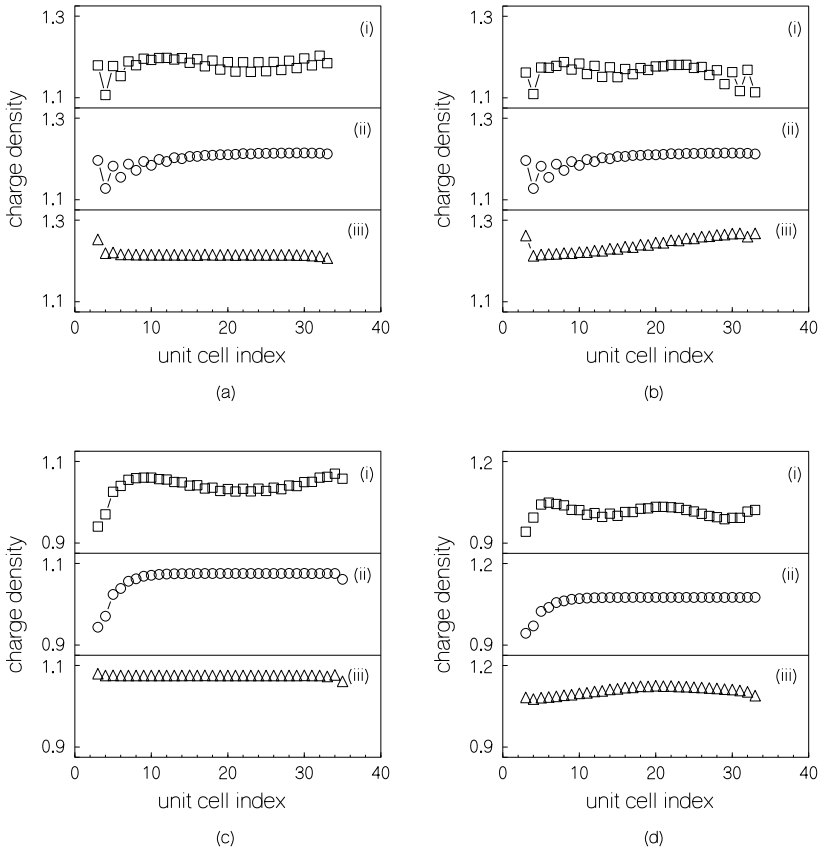

Figure 7. The charge density of a metal site versus the unit-cell index for a uniform MX chain. (a), (b) For polarons and bipolarons, respectively, for $U_M = 1.5t$, $U_X = 0.5t$, $\epsilon_M = 0$, and $\epsilon_X = -t$. (c), (d) For polarons and bipolarons, respectively, for $U_M = 2.5t$, $U_X = 0.5t$, $\epsilon_M = 0$, and $\epsilon_X = -2t$. (i) Positively charged (squares), (ii) neutral (circles), and (iii) negatively charged (triangles) systems, in all of the panels, (a)–(d).

The effect of site-diagonal distortion on the disproportionation is very dramatic. We compare the charge-density distribution for the positively charged polarons and bipolarons with (figure 9(b)) and without (figure 9(a)) site-diagonal distortion. In both cases, the localization of excess charge is confined to just one sublattice. In the system with site-diagonal distortion, the sublattice with nonuniform charge density is on the metal site for which the metal–halogen bond is long, corresponding to a negative ϵ_M, while in the absence of site-diagonal distortion, these metal sites have uniform charge distribution. This is seen as a changeover in the charge-density dips from the lower envelope in figure 9(a) to the upper envelope in figure 9(b). The changeover in the accommodation of excess charge upon introducing site-diagonal distortion is associated with the strong mixed-valence character introduced by nonzero ϵ_M. The disproportionation of the positively charged bipolaron is again found only for systems with large on-site repulsions, U_M.

The difference between MX chains at three-quarters filling and MX chains with one- and two-hole dopings can be seen clearly if the difference in charge density between corresponding metal sites of the neutral and doped chains is plotted as a function of the unit-cell index. We

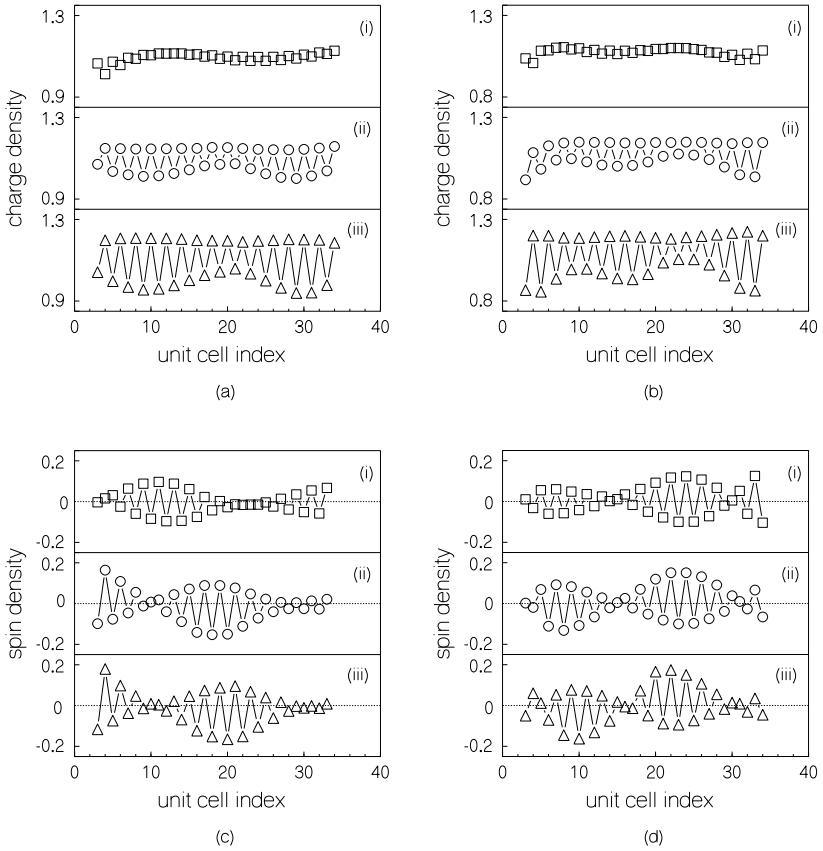

Figure 8. The charge density and spin density of a metal site for a positively doped MX chain for $U_M = 1.5t$, $U_X = 0.5t$, $\epsilon_M = 0$, and $\epsilon_X = -2t$. Charge densities for (a) polarons and (b) bipolarons. Spin densities for (c) polarons and (d) bipolarons. In all of the panels, (a)–(d), (i) $\delta = 0.0$ (squares), (ii) $\delta = 0.1$ (circles), and (iii) $\delta = 0.2$ (triangles).

show in figure 10 such difference plots for systems with site-diagonal distortion for weak- and strong-correlation cases. The envelopes of the charge-density distributions of the polaron and the bipolaron each show a single peak at small correlation strengths, while those for strong correlations each exhibit two distinct peaks for the bipolaron (figure 10(a), (iv)). A similar behaviour is found also in the spin-density distribution (figure 10(b), (iv)). The total charge under the peak is nearly the same for the positively charged polaron and bipolaron. This is because, in the bipolaron, part of the excess charge is accommodated uniformly on the halide ions, which is not shown in the figure.

The negatively charged bipolaron does not disproportionate even upon introducing the site-diagonal distortions. Apart from exhibiting mixed valency, the charge- and spin-density distributions are uniform on each sublattice.

The bond-order distributions in the negatively and positively charged bipolarons are almost similar to what is found in neutral chains. There is a tendency for the negatively charged bipolarons towards the elongation of the bonds (as seen from smaller bond orders in the middle of the chain), while the positively charged bipolarons have an opposite tendency, i.e., towards bond-length contraction. This agrees with an earlier study of the lattice distortions of doped

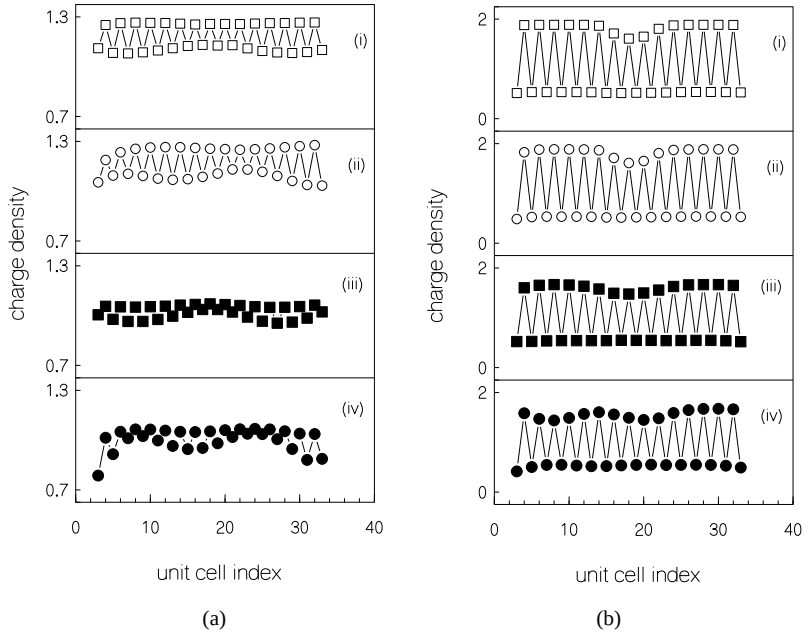

Figure 9. The charge density of a metal site for positively charged polarons (squares) and bipolarons (circles) for $U_X = 0.5t$ and $\delta = 0.1$. Open symbols are for $U_M = 1.5t$ and $\epsilon_X = -t$, and filled symbols are for $U_M = 2.5t$ and $\epsilon_X = -2t$; (a) for $\epsilon_M = 0.0$ and (b) for $\epsilon_M = t$.

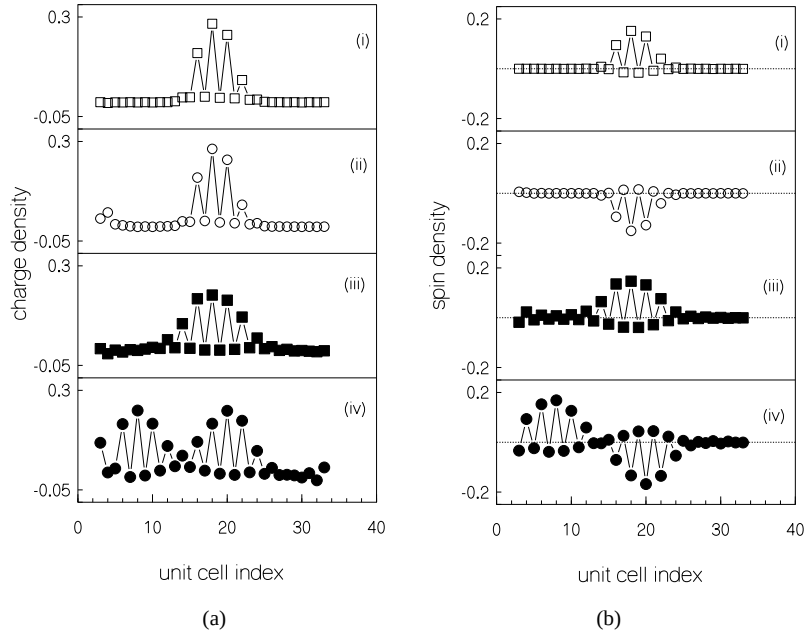

Figure 10. The difference in (a) charge density and (b) spin density of metal sites with respect to a neutral system for positively charged polarons and bipolarons for the same set of parameters as in figure 9 with the single $\epsilon_M = t$.

MX chains [3]. However, these marginal differences in the bond-order variations are reduced on introducing site-diagonal distortions.

The essential difference between the positively and negatively charged bipolarons lies in the disproportionation of the former into polarons in the strong-correlation limit, in the presence of alternation and site-diagonal distortion. From an analysis of the difference in bond orders between the neutral system and systems with one hole (electron) and two holes (electrons), we find that the system with one hole shows a tendency to distort in the middle of the chain while the two-hole system shows a tendency to have a spread in the bond-order difference. The dependence of the difference in bond order of negatively charged polarons and bipolarons are, however, very similar, and are consistent with a wide spread in the distortion that is predicted from other studies.

In summary, we have studied the phase diagram of MX chains within a two-band extended Peierls–Hubbard model employing the density-matrix renormalization group method. We find that the site energy associated with site-diagonal distortion is the single most important parameter for the transition from a SDW phase to a CDW phase in the ground state of the system. The variation of other parameters, such as the site energy of the halide site, the on-site Hubbard U of the halide ion, and bond alternations, do not change the nature of the ground state significantly. On the other hand, for the doped MX chains, both the bond alternation and the site-diagonal distortion play a major role. For positively doped systems, introduction of bond alternation leads to the localization of charge and spin densities. In the presence of site-diagonal distortion, we observe that the positively charged bipolaron disproportionates into two positively charged polarons in the strong-correlation limit. The negatively charged bipolarons do not show evidence for disproportionation even for the longest chain length and for the parameters that we have studied. We also find that there is a contraction of the bond length in the case of positively charged polarons and bipolarons, and elongation for the corresponding negatively charged species.

Acknowledgments

It is a pleasure to thank Professor H R Krishnamurthy for many fruitful discussions and Dr Biswadeb Dutta for system help.

References

[1] Tinka Gammel J, Donohoe R J, Bishop A R and Swanson B I 1990 *Phys. Rev.* B **42** 10 566
Tinka Gammel J, Saxena A, Batistic I, Bishop A R and Phillpot S R 1992 *Phys. Rev.* B **45** 6408
Weber-Milbrodt S M, Tinka Gammel J, Bishop A R and Loh E Y Jr 1992 *Phys. Rev.* B **45** 6435
[2] Mishima A and Nasu K 1989 *Phys. Rev.* B **39** 5758
Mishima A and Nasu K 1989 *Phys. Rev.* B **39** 5763
[3] Huang X Z and Bishop A R 1993 *Phys. Rev.* B **48** 16 148
[4] Tagawa Y and Suzuki N 1995 *J. Phys. Soc. Japan* **64** 1800
Tagawa Y and Suzuki N 1995 *J. Phys. Soc. Japan* **64** 2212
[5] Kuroda N, Sakai M, Nishina Y, Tanaka M and Kurita S 1987 *Phys. Rev. Lett.* **58** 2122
[6] Huang Q F, Wu C Q and Sun X 1995 *Phys. Rev.* B **52** 5637
[7] Girlando A, Painelli A and Ardoino M 1995 *Phys. Rev.* B **51** 17 338
[8] Haruki M and Kurita S 1983 *Phys. Rev.* B **39** 5706
[9] Okamoto H, Mitani T, Toriumi K and Yamashita M 1992 *Phys. Rev. Lett.* **69** 2248
[10] Nasu K 1983 *J. Phys. Soc. Japan* **52** 3865
[11] Nasu K 1984 *J. Phys. Soc. Japan* **53** 302
Nasu K 1984 *J. Phys. Soc. Japan* **53** 427
[12] Nasu K 1985 *J. Phys. Soc. Japan* **54** 1933

[13] Ichinose S 1984 *Solid State Commun.* **50** 137
[14] Onodera Y 1987 *J. Phys. Soc. Japan* **56** 250
[15] Baeriswyl D and Bishop A R 1988 *J. Phys. C: Solid State Phys.* **21** 339
[16] Anusooya Y and Ramasesha S 1994 *Proc. Indian Acad. Sci. (Chem. Sci.)* **106** 433
[17] Mishima A 1995 *Synth. Met.* **70** 1197
[18] Sun X, Yu Z G, Lee K H, Park T Y and Lin D L 1995 *Synth. Met.* **70** 1199
[19] Anisimov V I, Albers R C, Wills J M, Alouani M and Wilkins J W 1995 *Phys. Rev.* B **52** R6975
[20] White S R 1992 *Phys. Rev. Lett.* **69** 2863
White S R 1993 *Phys. Rev.* B **48** 10 345
[21] Ohno K 1964 *Theor. Chim. Acta* **2** 219
[22] Noack R M and White S R 1993 *Phys. Rev.* B **47** 9243
Pati S K, Chitra R, Sen D, Krishnamurthy H R and Ramasesha S 1996 *Europhys. Lett.* **33** 707
[23] Soos Z G and Ramasesha S 1990 *Valance Bond Theory and Chemical Structure* ed D J Klien and N Trinajstic (Amsterdam: Elsevier) p 81
[24] Rettrup S 1982 *J. Comput. Phys.* **45** 100
[25] Soos Z G and Ramasesha S 1984 *Phys. Rev.* B **29** 5410
[26] Sorenson E S and Affleck I 1995 *Phys. Rev.* B **49** 55 771